Five-band bias-selectable integrated quantum well detector in an *n-p-n* architecture

G. Ariyawansa,[1] Y. Aytac,[1] A. G. U. Perera,[1,a)] S. G. Matsik,[2] M. Buchanan,[3] Z. R. Wasilewski,[3] and H. C. Liu[3]
[1]*Department of Physics and Astronomy, Georgia State University, Atlanta, Georgia 30303, USA*
[2]*NDP Optronics LLC, Mableton, Georgia 30126, USA*
[3]*Institute for Microstructural Sciences, National Research Council, Ottawa, Ontario K1A 0R6, Canada*

(Received 12 October 2010; accepted 15 November 2010; published online 6 December 2010)

A detector with five bands covering visible to long-wave infrared is demonstrated using a GaAs-based *n-p-n*-architecture. The major elements are two back-to-back connected *p-i-n* photodiodes with InGaAs/GaAs and GaAs/AlGaAs-based quantum wells integrated within the *n*-regions. At 80 K, a preliminary detector shows two combinations of bands, each responding in three bands, covering the 0.6–0.8, 3–4, and 4–8 μm ranges and the 0.8–0.9, 0.9–1.0, and 9–13 μm ranges. A good selection of these two combinations based on the bias voltage polarity is observed. A similar four-band detector without any cross-talk between the bands is proposed using $In_{0.53}Ga_{0.47}As/InP$ material system. © *2010 American Institute of Physics*. [doi:10.1063/1.3524236]

With the development of infrared detector technology,[1] a significant effort has been put on developing multiband detectors, which are expected to show enhanced detection capabilities with reduced false positives. Already reported multiband detectors are based on HgCdTe, quantum well infrared photodetector (QWIP),[2,3] quantum dot infrared photodetector (QDIP),[4–6] and homo-/heterojunction[7,8] detector structures, and they cover visible (VIS), near-infrared (NIR), short-wave-infrared (SWIR), mid-wave-infrared (MWIR), and long-wave-infrared (LWIR). Although various approaches[3,4] are being studied to develop multiband detectors, not only the detection of light in multiple wavelength bands, but the selection of photocurrent components corresponding to each wavelength band should also be considered. Hence, there are new device physics concepts to discover.

Simultaneous-mode multiband detectors, in general, require more than two electrical contacts on the detector element, while two electrical contacts are adequate for sequential-mode multiband detectors.[3,6] In sequential-mode multiband detectors, two basic approaches are used to select the operating wavelength; (i) use of optical elements, such as filters, gratings, etc., and (ii) use of the applied bias voltage.[9,10] If the operating wavelength bands can be selected using the applied bias voltage, external optical components or electronics are not required for wavelength selection, giving an immense advantage over the existing multiband detectors. The use of bias voltage is based on the device architecture, band structure, photo- and dark-current transport mechanisms, and effects of the voltage on the band structure and carrier transport mechanisms. In this paper, a specific detector architecture that supports two or more detection mechanisms, which can be selected by the applied bias voltage, is discussed. The major elements in this detector architecture are two back-to-back connected *p-i-n* photodiodes, which is somewhat similar to the back-to-back *p-n* diode structure, which was demonstrated for HgCdTe dual-band detectors.[11] The carrier transport mechanisms are controlled by the characteristics of the back-to-back connected *p-i-n* architecture, which is identified as an *n-p-n* structure (two *p-i-n* regions connected as *n-i-p-i-n*), while IR detection is based on intersubband absorption in InGaAs/GaAs or GaAs/AlGaAs-based quantum wells (QWs), which are integrated within the *n*-regions of this complete structure referred to as *n-p-n*-QWIP.

The main idea of this detector architecture can be explained using two simple *p-i-n* photodiodes, which are assumed to respond in two bands (say, blue and red) and connected in series by connecting the *p*-type terminals. Then, the *n*-type layers on both sides are considered to be top (*n*-layer of the blue diode) and bottom (*n*-layer of the red diode) contacts. When a negative bias is applied to the top contact, the blue photodiode is under "forward" bias and the red photodiode is under "reverse" bias. Hence, under illumination, the dominant carrier transport in the blue photodiode is

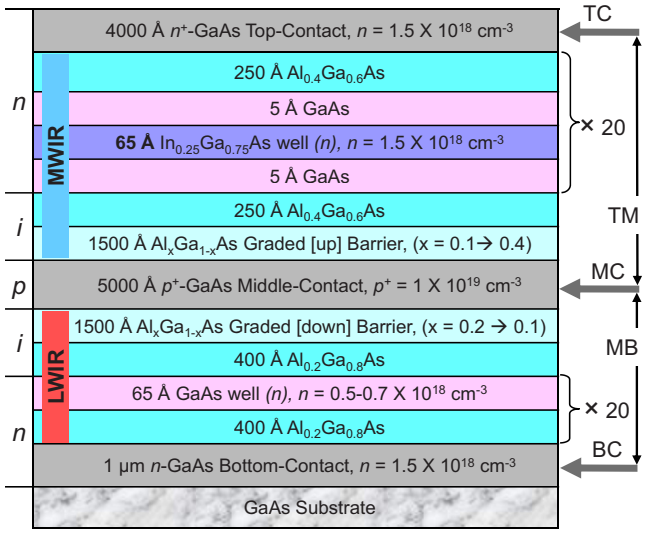

FIG. 1. (Color online) Schematic diagram of the *n-p-n*-QWIP (as-grown). Three doped layers (labeled TC, MC, and BC) separate two major active regions; one containing MWIR quantum wells (InGaAs) and the other containing LWIR quantum wells (GaAs). Three different measurement configurations (TM, MB, and TB) are also indicated.

a)Electronic mail: uperera@gsu.edu. Also at NDP Optronics LLC.

 © 2010 American Institute of Physics

Author complimentary copy. Redistribution subject to AIP license or copyright, see http://apl.aip.org/apl/copyright.jsp

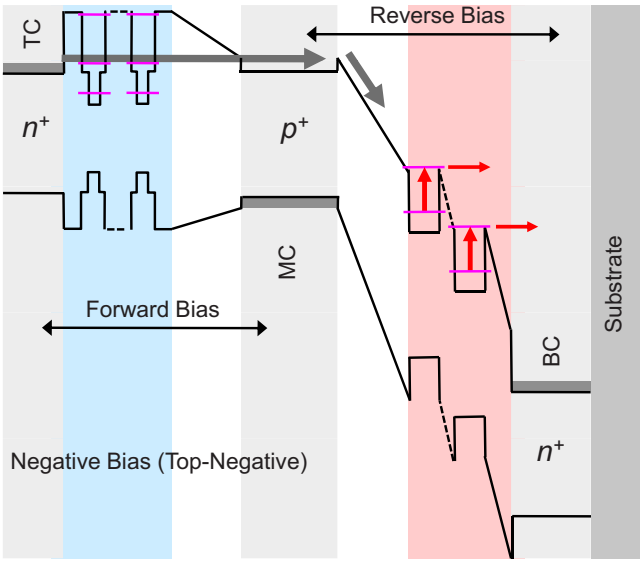

FIG. 2. (Color online) The conduction band profile of the detector for negative bias (negative on TC). Under this condition, the band profile of the TM region is close to the flat-band situation, making the MWIR wells inactive for photocarrier generation. Hence, photocarrier generation takes place only in the LWIR wells, as indicated by vertical arrows. Similarly, the MWIR well becomes active for positive bias.

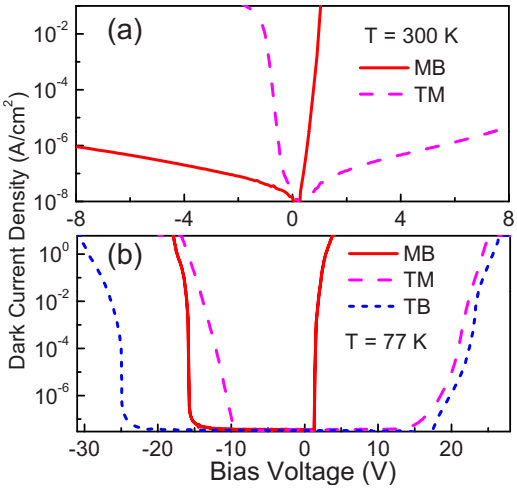

FIG. 3. (Color online) Dark current characteristics of the detector at (a) 300 K and (b) 77 K, measured across TM, MB, and TB. TM and MB regions separately show typical I-V characteristics of a *p-i-n* structure as expected. Three out of four mesas on this sample show very similar I-V, indicating a good uniformity.

through majority carriers (dark current), while the photoexcited carriers will generate a current in the red photodiode. Since the two diodes are in series, the net current will be determined by the photocurrent of the red photodiode. When a positive bias is applied to the top contact, the reverse process occurs and the net current is based on the photocurrent generated in the blue photodiode. That means one diode at a time can be activated for photocurrent generation by changing the bias voltage polarity.

The structure of the *n-p-n*-QWIP design tested in this study is shown in Fig. 1. The top, middle, and bottom contacts are labeled TC, MC, BC, respectively, while TM, MB, and TB indicate the three measurement configurations: top-middle, middle-bottom, and top-bottom, respectively. Although an ideal structure should have two electrical contacts, the present sample purposely had three electrical contacts with one in the middle *p*-doped layer in order to test the two active regions separately (i.e., the MC is only for testing purposes). In the following discussion, the bias polarity is identified as "positive" and "negative" when the contact layer, which is on the top of the region under consideration (TM, MB, or TB), is positively and negatively biased, respectively. As can be seen in Fig. 1, the TM and MB regions resemble a *p-i-n* type structure. The major difference between the two regions is that the TM consists of 20 periods of 65 Å thick InGaAs/GaAs/AlGaAs QWs to detect light in the 3–8 μm region (MWIR), while BM consists of 65 Å thick GaAs/AlGaAs QWs to detect light in the 8–14 μm region (LWIR).

The conduction and valence band profiles of the detector structure for negative bias (negative on the TC) are shown in Fig. 2. Under this condition, the band profile of the TM region is close to the flat-band situation, making the MWIR wells inactive for photocarrier generation. Hence, photocarrier generation takes place only in the LWIR wells, as indicated by vertical arrows. Similarly, the MWIR wells become active for positive bias. The ground state electrons are excited by the incoming photons and the excited electrons are collected as the photocurrent; however, the ground state should be refilled by electrons injected from the other end of the structure. Since the active *p-i-n*-region is under reverse condition, the major refilling mechanism would be through the leakage current. Hence, a high bias is required, and as is evident from the results for a QWIP in Ref. 2, a high response can be obtained if the magnitude of the bias is high enough to generate a current to refill the empty well states.

The dark current-voltage (I-V) characteristics of a mesa with an electrical area of 400×400 μm^2 at 300 K are shown in Fig. 3(a). The TM and MB regions show asymmetric I-V curves similar to a typical *p-i-n* structure (it should be noted that the TM region is under forward condition for negative bias and under reverse condition for positive bias, when it is compared with a typical *p-i-n* diode). However, when the temperature is reduced to 77 K, the two regions show different variations. This is attributed to the I-V characteristics of

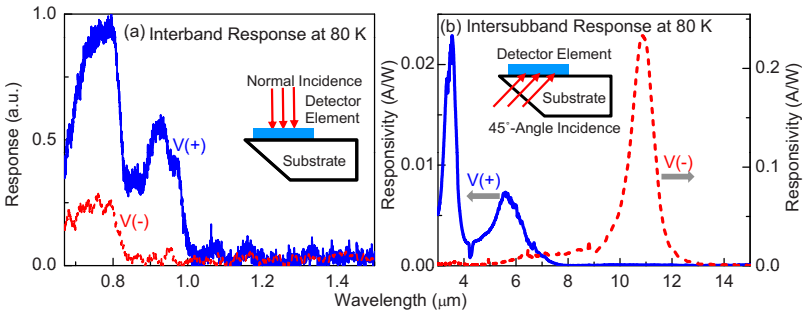

FIG. 4. (Color online) (a) Interband response of the *n-p-n*-QWIP measured with front-side illumination. (b) Intersubband spectral response measured with 45° back-side illumination at 80 K for positive (left scale) and negative (right scale) bias voltages indicated by V(+) and V(−). A good selection between the MWIR and LWIR bands can be observed. When this detector is coupled with a grating, both interband and intersubband responses can be measured with normal incidence light.

Author complimentary copy. Redistribution subject to AIP license or copyright, see http://apl.aip.org/apl/copyright.jsp

quantum wells. In general, at 80 K, the dark current[12] of short wavelength QWIPs is lower than that of long wavelength QWIPs. The response from the TM and MB regions was measured separately to confirm that the quantum wells respond in the expected wavelength ranges. However, the focus of this study is on the response and wavelength band selection capability across the TB region. In Fig. 4, the response of the detector due to interband and intersubband transitions is shown for positive (V+) and negative (V−) bias voltages. While interband response [Fig. 4(a)] will be discussed later, in Fig. 4(b) the response for positive bias is solely from the InGaAs/GaAs wells (MWIR) and the response for negative bias is solely from the GaAs/AlGaAs wells (LWIR). The two peaks observed at 3.6 and 6.0 μm match with the bound to bound transitions in the 65 Å thick InGaAs/GaAs wells in the TM region, while the peak at 10.8 μm is due to absorption in the GaAs/AlGaAs wells in the MB region, which is also in good agreement with theoretical predictions. It is also clear that the MWIR response is visible for positive bias, while the LWIR response is visible for negative bias, indicating a good selection between the two bands. This result is in good agreement with the detection and carrier collection mechanism in the *n-p-n*-QWIP architecture discussed before. The peak wavelengths can be changed by varying the well-width and the barrier alloy fractions, as in any other QWIPs. In addition, almost zero spectral cross-talk between the two bands was observed for a deviation of ±2 V from both positive and negative bias values shown in Fig. 4. The measured detectivity (D^*) values at 80 K are $\sim 2\times 10^8$ and 5×10^9 at 3.6 and 10.8 μm, respectively. Although these values are lower than the D^* values of typical QWIPs, they can be increased by optimizing the layer parameters in the *n-p-n*-structure considering the transport of dark and photocarriers.

In addition, the interband response shown in Fig. 4(a) further justifies the mechanism in the *n-p-n*-QWIP structure. Under negative bias (see Fig. 2), interband absorption in the MB region, which is the active region under negative bias, leads to a response in the VIS-NIR range. The wavelength threshold (~0.82 μm) corresponds to the smallest transition energy in the MB region, which is the band gap of the GaAs layer. Similarly, under positive bias, the TM region becomes active and interband transitions take place in the InGaAs layers, as well as in the GaAs layers, leading to a response band in VIS-NIR-SWIR range with two wavelength thresholds at ~0.82 and ~1 μm, respectively. Within the wavelength range specified, the average interband absorption coefficient is approximately 5×10^4 cm^{-1}, which translates to a skin depth of 0.2 μm. This indicates that most of the VIS-NIR light is absorbed within the top layers. Hence, the interband response can be further enhanced by etching out the top-contact layer inside the metal ring. The overall result in Fig. 4 indicates that the detector can be operated as a VIS-NIR+SWIR+MWIR detector with positive bias and a VIS-NIR+LWIR detector with negative bias.

The interband (VIS-NIR) spectral cross-talk observed for the GaAs-based *n-p-n*-QWIP can be reduced using a material system such as $In_{0.53}Ga_{0.47}As/InP$ in an *n-p-n*-QWIP structure. Specific elements in an $In_{0.53}Ga_{0.47}As/InP$-based *n-p-n*-QWIP structure and corresponding spectral bands expected from these elements are shown in Table I. Since light at wavelengths below 0.9 μm will be absorbed in the top InP layers, the *i*-$In_{0.53}Ga_{0.47}As$ layer will respond to light only in the 0.9–1.7 μm range (1.7 μm corresponds to the band gap of $In_{0.53}Ga_{0.47}As$). The VIS-NIR and MWIR bands can be selected using a positive bias on the top contact, while the SWIR and LWIR bands can be selected using a negative bias on the top contact.

TABLE I. Active elements in an $In_{0.53}Ga_{0.47}As/InP$-based *n-p-n*-QWIP.

Layer material	Response wavelength band	Bias
n-InP TC	VIS-NIR, 0.4–0.9 μm (Interband)	+ve
i-InP	VIS-NIR, 0.4–0.9 μm (Interband)	+ve
p-$In_{0.53}Ga_{0.47}As/InP$ Quantum wells	MWIR, 3–5 μm (Intersubband)	+ve
p-$In_{0.53}Ga_{0.47}As$	SWIR, 0.9–1.2 μm (Interband)	−ve
i-$In_{0.53}Ga_{0.47}As$	SWIR, 0.9–1.2 μm (Interband)	−ve
n-$In_{0.53}Ga_{0.47}As/InP$ Quantum wells	LWIR, 7–12 μm (Intersubband)	−ve
n-InP BC		
InP substrate		

In summary, a bias-selectable multicolor detector was demonstrated based on a GaAs-based *n-p-n*-QWIP. A four-band *n-p-n*-QWIP detector using the $In_{0.53}Ga_{0.47}As/InP$ material system was also proposed. This work was supported, in part, by the U.S. Air Force, under the STTR Contract Nos. FA9550-09-C-0106 and FA9550-10-C-0131, and the Georgia Research Alliance.

[1] A. Rogalski, J. Antoszewski, and L. Faraone, J. Appl. Phys. **105**, 091101 (2009).
[2] G. Ariyawansa, P. V. V. Jayaweera, A. G. U. Perera, S. G. Matsik, M. Buchanan, Z. R. Wasilewski, and H. C. Liu, Opt. Lett. **34**, 2036 (2009).
[3] A. Majumdar, K. K. Choi, J. L. Reno, and D. C. Tsui, Appl. Phys. Lett. **86**, 261110 (2005).
[4] G. Ariyawansa, V. Apalkov, A. G. U. Perera, S. G. Matsik, G. Huang, and P. Bhattacharya, Appl. Phys. Lett. **92**, 111104 (2008).
[5] H. C. Liu, M. Gao, J. McCaffrey, Z. R. Wasilewski, and S. Fafard, Appl. Phys. Lett. **78**, 79 (2001).
[6] G. Ariyawansa, A. G. U. Perera, G. Huang, and P. Bhattacharya, Appl. Phys. Lett. **94**, 131109 (2009).
[7] G. Ariyawansa, M. B. M. Rinzan, D. G. Esaev, S. G. Matsik, G. Hastings, A. G. U. Perera, H. C. Liu, B. N. Zvonkov, and V. I. Gavrilenko, Appl. Phys. Lett. **86**, 143510 (2005).
[8] R. C. Jayasinghe, G. Ariyawansa, N. Dietz, A. G. U. Perera, S. G. Matsik, H. B. Yu, I. T. Ferguson, A. Bezinger, S. R. Laframboise, M. Buchanan, and H. C. Liu, Opt. Lett. **33**, 2422 (2008).
[9] S. Krishna, D. Forman, S. Annamalai, P. Dowd, P. Varangis, T. Tumolillo, Jr., A. Gray, J. Zilko, K. Sun, M. Liu, J. Campbell, and D. Carothers, Appl. Phys. Lett. **86**, 193501 (2005).
[10] S. V. Bandara, S. D. Gunapala, J. K. Liu, S. B. Rafol, C. J. Hill, D. Z. Y. Ting, J. M. Mumolo, T. Q. Trinh, J. M. Fastenau, and A. W. K. Liu, Appl. Phys. Lett. **86**, 151104 (2005).
[11] E. Smith, L. Pham, G. Venzor, E. Norton, M. Newton, P. Goetz, V. Randall, A. Gallagher, G. Pierce, E. Patten, R. Coussa, K. Kosai, W. Radford, L. Giegerich, J. Edwards, S. Johnson, S. Baur, J. Roth, B. Nosho, T. De Lyon, J. Jensen, and R. Longshore, J. Electron. Mater. **33**, 509 (2004).
[12] H. Schneider and H. C. Liu, *Quantum Well Infrared Photodetectors: Physics and Applications* (Springer, New York, 2007).

Author complimentary copy. Redistribution subject to AIP license or copyright, see http://apl.aip.org/apl/copyright.jsp